THE BELL SYSTEM TECHNICAL JOURNAL
Vol. 62, No. 1, January 1983
Printed in U.S.A.

Maximum-Power and Amplitude-Equalizing Algorithms for Phase Control in Space Diversity Combining

By P. D. KARABINIS

(Manuscript received October 12, 1981)

Space diversity receivers equipped with continuous combiners have, in recent years, found wide use in terrestrial microwave radio systems as a means of mitigating the effects of multipath fading. An analysis of two phase-control algorithms for space diversity combining, comparing the performance capabilities of a maximum-power and an amplitude-equalizing algorithm, is presented in this paper. The extended capabilities of the equalizing algorithm in mitigating linear and quadratic channel distortions are investigated through computer simulations. A reduction in digital radio outage time afforded by the equalizing algorithm (relative to that of the maximum-power algorithm) is approximated for over-water-paths where it is assumed that fading can be described in terms of a two-ray fading model. For the model chosen, we show that the additional outage reduction owing to the equalizing phase-control algorithm is highly dependent on the statistics of the multipath delay parameter, τ, and can vary from unity to a factor of five for different probability-density functions of τ.

I. INTRODUCTION AND SUMMARY

High-speed digital radio systems operating in the 4-, 6-, and 11-GHz common-carrier bands experience severe performance degradations during periods of multipath fading.[1-7] These degradations are mainly due to intersymbol interference resulting from dispersive channel characteristics (amplitude and group-delay distortions) that typically accompany multipath fading.

Space diversity reception with continuous combining of the received signals has proven very effective in mitigating the amplitude and group-delay distortions caused by multipath fading.[4,5] Traditionally, maximum combined-signal power has been used as the control crite-

rion for combining the received signals.[8] Although maximum-power combining does not react to inband dispersion directly, the method does provide a substantial statistical improvement in this respect. In general, however, the output signal of a maximum-power combiner during dispersive fading will contain, to some degree, linear and quadratic amplitude distortion, with the linear component usually being the predominant one.[4,8] Because of this, the use of an amplitude slope equalizer following a maximum-power combiner has proven very effective in reducing the multipath outage of high-speed digital radio signals to levels compatible with long-haul outage objectives.[4]

With the advent of higher-level digital-modulation formats, equalization requirements of microwave radio channels are becoming increasingly stringent.[9] To optimize the performance of space diversity combiners used in modern digital radio systems, alternate phase-control algorithms have recently been proposed that depart from the traditional maximum-power algorithm in that, instead of maximum combined-signal power, minimum combined-signal dispersion becomes the controlling criterion.[10,11] With these equalizing phase-control algorithms, space diversity combiners have been shown to provide reduced levels of signal dispersion during periods of multipath fading[7] (as compared with maximum-power combiners), thus further reducing the multipath-related outage of high-speed digital signals. One such equalizing algorithm is proposed, analyzed, and compared with a maximum-power algorithm in this paper.

In Section II, the conventional maximum-power combiner is reviewed first, with a particular implementation of the maximum-power phase-control algorithm described in detail. Then we show how the maximum-power algorithm can be converted into an equalizing algorithm by judiciously extracting a phase-control signal from selected portions of the combined-signal spectrum. The analysis reveals that the maximum-power algorithm is only a special case of a more general algorithm that can adaptively maximize the combined-signal power over any frequency interval in the channel. The particular equalizing phase-control algorithm described minimizes the power difference between two spectral samples derived symmetrically from the upper and lower portions of the combined-signal spectrum. To achieve this, the algorithm maximizes the power of the upper or lower spectral sample (as determined by a control criterion) and attempts to bring the two frequency subbands in power equilibrium. As a consequence, we show that the linear and quadratic amplitude distortions of the combined-signal spectrum are substantially reduced for many dispersive channel conditions.

Section III presents results of computer simulations illustrating the response of the maximum-power and equalizing combiners to disper-

sive channel conditions. An improvement factor of the equalizing combiner over the maximum-power combiner is calculated for several assumed probability-density functions of the parameters of a two-ray fading model. Since a two-ray fading model is more likely to represent fading accurately for microwave radio paths over water (where a strong reflective component is typically present during fading) our results too should be viewed in that context. For microwave radio paths over land, it has been shown by Rummler[12] that a three-ray model is required to accurately describe multipath fading. For the two-ray model chosen here, we show that the equalizing combiner improvement factor is strongly dependent on the assumed probability-density function of the multipath delay parameter τ and varies from approximately unity (no improvement) to a factor of five, for different probability-density functions of τ and expected values of τ.

II. MAXIMUM-POWER AND AMPLITUDE-EQUALIZING PHASE-CONTROL ALGORITHMS

A simplified block diagram of a space diversity receiver providing two signal inputs to a continuous combiner is shown in Fig. 1. Following a fixed delay adjustment of the diversity-signal path (to equalize the

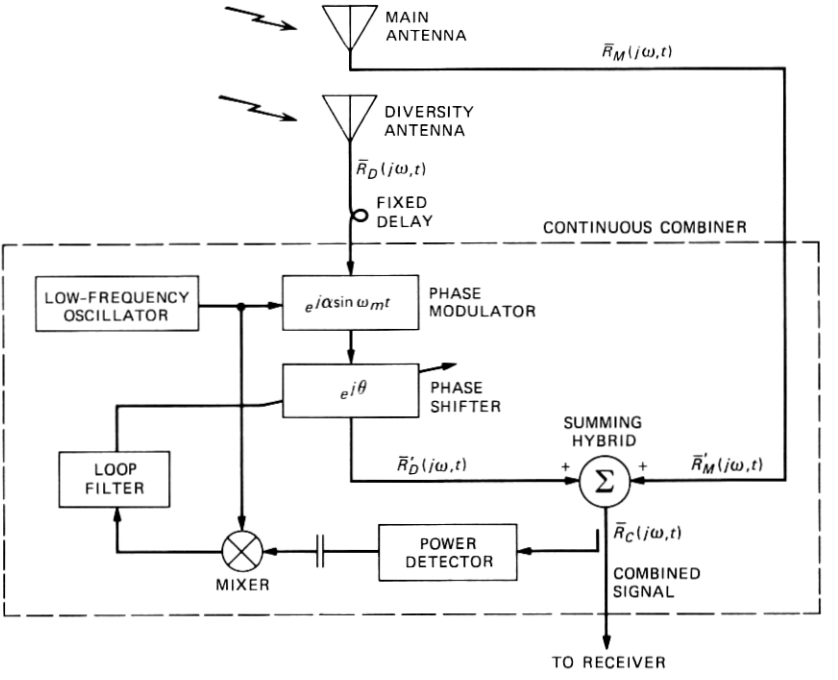

Fig. 1—Block diagram of a space diversity continuous combiner.

electrical path lengths leading to the combiner inputs), the phase of the diversity signal undergoes a dynamic adjustment so as to always maintain the proper relationship with respect to the main-antenna signal phase at the summing hybrid. For the purpose of generating a phase-control signal, the phase of the diversity antenna signal is perturbed sinusoidally, resulting in a periodic modulation of the combined-signal power.[13] The fundamental component of the combined-signal power modulation is detected and used in a feedback arrangement to control the phase-shifter value.[14] Depending on the phase-control algorithm used, the phase correction can be chosen to maximize the average combined-signal power or minimize the dispersion of the combined signal.

In the appendix, the combined-signal power modulation resulting from the sinusoidal phase modulation of the diversity antenna signal is calculated in terms of the spectral densities and phase misalignment of the antenna signals at the inputs of the summing hybrid. In Section 2.1 below we show how the fundamental component of the combined-signal power modulation can be used as the control signal in a simple feedback loop to form a maximum-power combining algorithm. Section 2.2 describes a method of converting the maximum-power combiner of Section 2.1 into an equalizing combiner by selectively extracting the combined-signal power modulation from two frequency bands symmetrically located to the left and right of the channel center frequency.

2.1 Maximum-power phase-control algorithm

The average combined-signal power over the entire channel can be expressed, using eqs. (44) through (46) of the appendix, as:

$$p_0(t, \theta) = \frac{1}{2\pi}\int_{\omega_1}^{\omega_2} \delta^2(\omega, t)V^2(\omega, t)d\omega + \frac{1}{2\pi}\int_{\omega_1}^{\omega_2} V^2(\omega, t)d\omega + \frac{1}{\pi}J_0(\alpha)\int_{\omega_1}^{\omega_2} \delta(\omega, t)V^2(\omega, t)\cos\{\psi(\omega, t) + \theta\}d\omega, \quad (1)$$

where the frequency interval $\omega_1 \leq \omega \leq \omega_2$ is assumed to span the channel bandwidth, $\delta^2(\omega, t)V^2(\omega, t)$ and $V^2(\omega, t)$ denote the diversity and main antenna power-spectral densities, respectively, $\psi(\omega, t)$ is the phase of the diversity antenna spectrum relative to the phase of the main antenna spectrum before any phase correction, θ represents the frequency-independent phase correction introduced in the diversity antenna spectrum by the phase shifter (see Fig. 1), and $J_0(\alpha)$ denotes a Bessel function of the first kind whose argument is the magnitude of the sinusoidal phase modulation introduced in the diversity signal. The explicit dependence of the variables appearing in eq. (1) on time

accounts for slow variations of these parameters caused by changes in the transmission medium. However, these variations are assumed quasi-static with respect to the transmission rate of the microwave radio channel.

To find θ_m, the value of θ that maximizes $p_0(t, \theta)$, we set the first partial derivative of $p_0(t, \theta)$ to zero and require the second partial derivative to be negative. That is,

$$\left.\frac{\partial p_0(t, \theta)}{\partial \theta}\right|_{\theta=\theta_m} = -\frac{1}{\pi} J_0(\alpha) \int_{\omega_1}^{\omega_2} \delta(\omega, t) V^2(\omega, t) \sin\{\psi(\omega, t) + \theta_m\} d\omega = 0 \quad (2)$$

and

$$\left.\frac{\partial^2 p_0(t, \theta)}{\partial \theta^2}\right|_{\theta=\theta_m} = -\frac{1}{\sqrt{2}\pi} J_0(\alpha) \int_{\omega_1}^{\omega_2} \delta(\omega, t) V^2(\omega, t) \cos\{\psi(\omega, t) + \theta_m\} d\omega < 0. \quad (3)$$

Having established the conditions for maximum-power combining, we will now show that the phase-control loop of Fig. 2 finds a value of θ that satisfies these conditions.

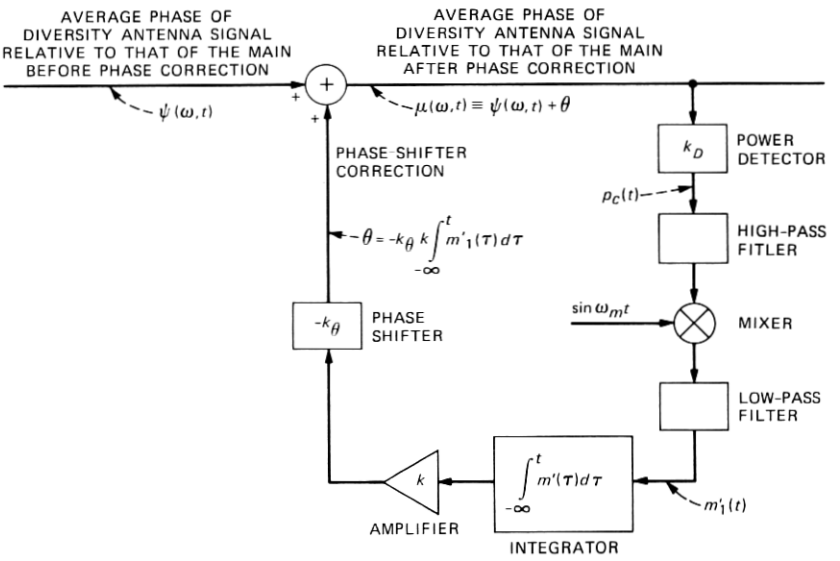

Fig. 2—Block diagram of maximum-power combiner phase-control loop.

From the assumption of a slowly varying transmission medium, the fundamental component of the combined-signal power modulation, $m_1'(t)$, [derived in the appendix, eq. (55)] will be a narrowband process. Choosing the corner frequencies of the high-pass and low-pass filters of Fig. 2 well below and above the highest spectral component of $m_1'(t)$, respectively, the function $m_1'(t)$ will be unaffected by these filters.* Therefore, from an examination of the phase-control loop of Fig. 2 we can write:

$$\theta = -k_\theta k \int_{-\infty}^{t} m_1'(\tau)d\tau, \tag{4}$$

where k and $-k_\theta$ denote component gains as shown in Fig. 2. The rate of change of θ with respect to time can be expressed from eq. (4) and eqs. (55) and (49) of the appendix as

$$\frac{d\theta}{dt} = -k_\theta k m_1'(t)$$

$$= -4J_1(\alpha)k_\theta k \frac{\int_{\omega_1}^{\omega_2} \delta(\omega, t)V^2(\omega, t)\sin\{\psi(\omega, t) + \theta\}d\omega}{\int_{\omega_1}^{\omega_2} V_{co}^2(\omega, t)d\omega}. \tag{5}$$

Observe from eq. (5) that a nonchanging value of θ can exist if and only if

$$m_1'(t) = \frac{4J_1(\alpha)\int_{\omega_1}^{\omega_2} \delta(\omega, t)V^2(\omega, t)\sin\{\psi(\omega, t) + \theta\}d\omega}{\int_{\omega_1}^{\omega_2} V_{co}^2(\omega, t)d\omega} = 0, \tag{6}$$

which implies that

$$\int_{\omega_1}^{\omega_2} \delta(\omega, t)V^2(\omega, t)\sin\{\psi(\omega, t) + \theta\}d\omega = 0. \tag{7}$$

Therefore, if $m_1'(t) \neq 0$ the phase shifter correction, θ, will continue to change until a value satisfying eq. (7) is found. In satisfying eq. (7), eq. (2) and, therefore, the first condition for maximum-power combining is simultaneously satisfied. It remains to be shown that this value of

* It is also assumed that the modulation frequency ω_m is large compared with the bandwidth of $m_1'(t)$. For example, if the bandwidth of $m_1'(t)$ is limited to 1 Hz, then we choose $f_m = (\omega_m/2\pi) \geq 10$ Hz.

θ also satisfies the second condition for maximum-power combining as expressed by inequality (3).

Assume that a value of θ, $\theta = \theta_0$, satisfying eq. (7) is found by the phase-control loop. That is, assume an initial condition of $\theta = \theta_0 \pm \Delta\theta$, $\Delta\theta > 0$, and a final condition of $\theta = \theta_0$. With $\theta = \theta_0 \pm \Delta\theta$ we have

$$\int_{\omega_1}^{\omega_2} \delta(\omega, t) V^2(\omega, t) \sin\{\psi(\omega, t) + \theta_0 \pm \Delta\theta\} d\omega \neq 0. \tag{8}$$

Defining,

$$\begin{aligned} \xi &\equiv \int_{\omega_1}^{\omega_2} \delta(\omega, t) V^2(\omega, t) \sin\{\psi(\omega, t) + \theta_0 \pm \Delta\theta\} d\omega \\ &= \frac{\int_{\omega_1}^{\omega_2} V_{co}^2(\omega, t) d\omega}{4J_1(\alpha)} m_1'(t), \end{aligned} \tag{9}$$

ξ may be expressed as

$$\begin{aligned} \xi = \cos(\pm\Delta\theta) &\int_{\omega_1}^{\omega_2} \delta(\omega, t) V^2(\omega, t) \sin\{\psi(\omega, t) + \theta_0\} d\omega \\ + \sin(\pm\Delta\theta) &\int_{\omega_1}^{\omega_2} \delta(\omega, t) V^2(\omega, t) \cos\{\psi(\omega, t) + \theta_0\} d\omega. \end{aligned} \tag{10}$$

Since by assumption, the first term of eq. (10) is zero we are left with

$$\begin{aligned} \xi &= \sin(\pm\Delta\theta) \int_{\omega_1}^{\omega_2} \delta(\omega, t) V^2(\omega, t) \cos\{\psi(\omega, t) + \theta_0\} d\omega \\ &= \frac{\int_{\omega_1}^{\omega_2} V_{co}^2(\omega, t) d\omega}{4J_1(\alpha)} m_1'(t). \end{aligned} \tag{11}$$

If the assumed θ increment is taken positive ($+\Delta\theta$) the integral of eq. (11), $\int_{\omega_1}^{\omega_2} \delta(\omega, t) V^2(\omega, t) \cos\{\psi(\omega, t) + \theta_0\} d\omega$, must be positive to make $m_1'(t)$ positive. A positive $m_1'(t)$ will generate a negative $d\theta/dt$ [see eq. (5)] as is required to force $\theta = \theta_0 + \Delta\theta$ to $\theta = \theta_0$, as per assumption. Otherwise, $\theta = \theta_0 + \Delta\theta$ will migrate away from $\theta = \theta_0$, contradicting the initial assumption. Similarly, if we assume a negative θ increment ($-\Delta\theta$) the integral $\int_{\omega_1}^{\omega_2} \delta(\omega, t) V^2(\omega, t) \cos\{\psi(\omega, t) + \theta_0\} d\omega$ must again be positive in order for a positive $d\theta/dt$ to be generated as is required to force $\theta = \theta_0 - \Delta\theta$ to $\theta = \theta_0$.

Having shown that $d\theta/dt = 0$ if and only if $m_1'(t) = 0$ (which requires

that $\int_{\omega_1}^{\omega_2} \delta(\omega, t)V^2(\omega, t)\sin\{\psi(\omega, t) + \theta_0\}d\omega = 0)$, in conjunction with $d\theta/dt = 0$ if and only if $\int_{\omega_1}^{\omega_2} \delta(\omega, t)V^2(\omega, t)\cos\{\psi(\omega, t) + \theta_0\}d\omega > 0$, we have shown that the phase-control loop of Fig. 2 satisfies both conditions for maximum-power combining.

2.2 Amplitude-equalizing phase-control algorithm

In the previous section we showed that the phase-control loop of Fig. 2 finds a phase shifter value that forces the fundamental component of the combined-signal power modulation, $m_1'(t)$, to zero over the frequency interval $\omega_1 \leq \omega \leq \omega_2$, and in doing so, also maximizes the average combined-signal power over the same frequency interval. Therefore, when $\omega_1 \leq \omega \leq \omega_2$ spans the entire channel bandwidth, as is the case in Fig. 2 (where the combined-signal spectrum is allowed to be seen in its entirety by the power detector), the combined-signal power will be maximized over the entire channel. However, if a narrowband filter is inserted before the power detector of Fig. 2, allowing only a fraction of the combined-signal spectrum to be seen by the power detector, the combined-signal power will be maximized over the frequency band seen by the power detector and not necessarily over the entire channel bandwidth, since the phase difference between the received spectra will, in general, be frequency dependent during periods of multipath fading.

In this section we will examine a more general version of the phase-control loop of Fig. 2, where the signal at the power-detector input is a filtered version of the combined-signal spectrum. Specifically, we will show that an equalizing phase-control algorithm, which minimizes the amplitude slope across the combined-signal spectrum, can be derived from the phase-control loop of Fig. 2 by requiring that the power detector input signal be a weighted sum of spectral components derived symmetrically from the left and right portions of the combined-signal spectrum.

Consider Fig. 3 where two narrowband portions of the combined-signal spectrum, each occupying a bandwidth $2\,\Delta\omega$ and centered at ω_l and ω_r, respectively, are extracted by the two narrowband filters. The center frequencies of the narrowband filters, ω_l and ω_r, are equally spaced from the center of the channel and are located to the left and right of the channel center-frequency, respectively. From the output signal of each narrowband filter, a power detector generates a voltage proportional to the combined-signal power found within the corresponding frequency interval, $\omega_l - \Delta\omega \leq \omega \leq \omega_l + \Delta\omega$ and $\omega_r - \Delta\omega \leq \omega \leq \omega_r + \Delta\omega$. Denoting the power detector output voltages by $p_l(t)$ and $p_r(t)$, corresponding to frequency intervals $\omega_l - \Delta\omega \leq \omega \leq \omega_l + \Delta\omega$ and $\omega_r - \Delta\omega \leq \omega \leq \omega_r + \Delta\omega$, respectively, the development in the appendix can be used to express $p_l(t)$ and $p_r(t)$ as

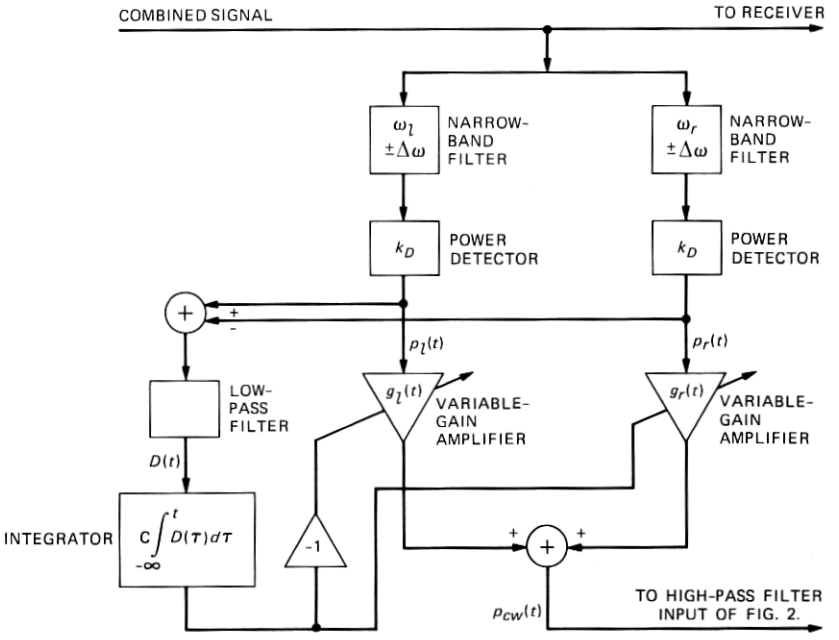

Fig. 3—Power detector portion of equalizing-combiner phase-control loop.

$$p_l(t) = k_D p_{0l}(t)[1 - m'_{1l}(t)\sin \omega_m t + m'_{2l}(t)\cos 2\omega_m t - \cdots] \quad (12)$$

and

$$p_r(t) = k_D p_{0r}(t)[1 - m'_{1r}(t)\sin \omega_m t + m'_{2r}(t)\cos 2\omega_m t - \cdots], \quad (13)$$

where k_D is a proportionality constant associated with each power detector (two identical power detectors are assumed) and with all other variables, $p_{0l}(t)$, $p_{0r}(t)$, $m'_{1l}(t)$, $m'_{1r}(t)$, $\cdots$, conforming to eqs. (52) through (54) of the appendix.

The power detector outputs, $p_l(t)$ and $p_r(t)$, are weighted by variable-gain amplifiers and then summed. Thus, a voltage, $p_{cw}(t)$, representing a weighted combined-signal power over the channel is derived (see Fig. 3), and can be expressed as

$$p_{cw}(t) = g_l(t)p_l(t) + g_r(t)p_r(t). \quad (14)$$

The weighting gains, $g_l(t)$ and $g_r(t)$, are determined by the integral of a difference function, $D(t)$, which is proportional to the average power difference between the frequency bands $\omega_l - \Delta\omega \leq \omega \leq \omega_l + \Delta\omega$ and $\omega_r - \Delta\omega_r \leq \omega \leq \omega_r + \Delta\omega$. That is, we let

$$D(t) \equiv k_D[p_{0l}(t) - p_{0r}(t)], \quad (15)$$

$$g_l(t) \equiv -k_g C \int_{-\infty}^{t} D(\tau)d\tau, \tag{16}$$

and

$$g_r(t) \equiv k_g C \int_{-\infty}^{t} D(\tau)d\tau, \tag{17}$$

where k_g is a proportionality constant associated with the variable-gain amplifiers and C is an integration constant. In addition, we require that the gains $g_l(t)$ and $g_r(t)$ be bounded

$$\left.\begin{aligned} 0 \le g_l(t) \le g_{\max} \\ 0 \le g_r(t) \le g_{\max} \end{aligned}\right\} \text{ for all } t. \tag{18}$$

It can now be seen from eqs. (15) through (17) that if a positive amplitude slope exists across the combined-signal spectrum, $p_{0r}(t) > p_{0l}(t)$, $D(t)$ will be negative causing $g_l(t)$ to increase [or remain fixed at $g_{\max}$ if, initially, $g_l(t) = g_{\max}$] and $g_r(t)$ to decrease [or remain fixed at zero if, initially, $g_r(t) = 0$]. That is,

$$\begin{aligned} &\text{if } p_{0r}(t) > p_{0l}(t) \\ &\text{(positive amplitude slope)} \end{aligned} \qquad \text{then:} \quad \begin{cases} \dfrac{dg_l(t)}{dt} \ge 0 \\ \dfrac{dg_r(t)}{dt} \le 0. \end{cases} \tag{19}$$

Similarly, if a negative slope exists across the combined-signal spectrum, $p_{0r}(t) < p_{0l}(t)$, $D(t)$ will be positive causing $g_l(t)$ to decrease (or remain fixed at zero) and $g_r(t)$ to increase (or remain fixed at $g_{\max}$). Therefore:

$$\begin{aligned} &\text{if } p_{0r}(t) < p_{0l}(t) \\ &\text{(negative amplitude slope)} \end{aligned} \qquad \text{then:} \quad \begin{cases} \dfrac{dg_l(t)}{dt} \le 0 \\ \dfrac{dg_r(t)}{dt} \ge 0. \end{cases} \tag{20}$$

As the integration constant C [appearing in eqs. (16) and (17)] increases, the response of $p_{cw}(t)$ to a changing amplitude slope becomes faster. In the limit, as C approaches infinity, $p_{cw}(t)$ can assume only two values: either $g_{\max} p_l(t)$ or $g_{\max} p_r(t)$ corresponding to $D(t) < 0$ and $D(t) > 0$, respectively. That is, $p_{cw}(t)$ will instantaneously reflect the power-detector voltage corresponding to the weaker side of the combined-signal spectrum. Thus, with C very large, substituting the block diagram of Fig. 3 in place of the power detector of Fig. 2 results in a

phase-control loop that will always maximize the power of the weaker portion of the combined-signal spectrum and, therefore, minimize the amplitude slope across the combined-signal spectrum.

In the absence of dispersive channel conditions, the amplitude slope of the combined-signal spectrum will be zero. During such periods, random noise effects will dictate the value of $D(t)$. This, however, is of no consequence since in the absence of channel dispersion the phase difference between the received spectral densities is frequency independent and, therefore, maximizing the combined-signal power over any frequency interval within the channel necessarily maximizes the combined-signal power over the entire channel. Consequently, during dispersion-free periods, the equalizing phase-control algorithm described above becomes indistinguishable from the maximum-power phase-control algorithm.

In the following section, results of computer simulations, illustrating the relative performance capabilities of the maximum-power and amplitude-equalizing phase-control algorithms during dispersive channel conditions, are presented.

III. RELATIVE PERFORMANCE OF MAXIMUM-POWER AND AMPLITUDE-EQUALIZING PHASE-CONTROL ALGORITHMS

The algorithms described above have been stressed by computer simulations using a two-ray fading model. The fade parameters of the model, relative amplitude and delay, are treated as independent random variables and are assigned physical significance. That is, the model adopted here differs from that of Rummler's[12] where the delay parameter τ is assigned mathematical significance only and treated as a constant. Following the approach of Jakes[3] and Greenstein and Prabhu[15] we assume an exponential form for the probability-density function of the delay parameter τ. For comparison purposes we also examine other forms of the probability-density function of τ, including a Gaussian probability-density function.[16] The probability-density function of the relative amplitude of the delayed wavefront is assumed constant for deep fades.[3,15,16]

To facilitate the simulation of the space diversity arrangement of Fig. 1, we adopt a ray-optical view of wave propagation,[17-19] and assume a circular trajectory for the delayed wavefront. These assumptions enable one to calculate the fade on the diversity antenna given the fade on the main antenna. However, for a given fade-notch location on the main antenna, the fade-notch location on the diversity antenna will in practice be distributed over a wide frequency range since there are many physical τ's that can generate a particular fade-notch location on the main antenna. Each one of these τ's will generate a fade notch on the diversity antenna at a different frequency (because of the

geometry of the space diversity arrangement), thus giving the appearance of independent fading between the two antennas.

The receiving antennas are assumed identical and spaced vertically by 30 feet. The channel bandwidth is set at 30 MHz, centered at an RF frequency of 6 GHz, and propagation is assumed over a hop length of 26.4 miles. Finally, all fades seen by the two antennas are assumed, for simplicity, to be of the minimum-phase type.

The space diversity channel model resulting from the above assumptions provides a tractable means of generating a set of stressing simulated fade conditions. The results generated by these simulations are to be viewed as first-order approximations only, until such time as other analytical methods are developed allowing for alternate, perhaps more accurate, channel descriptions.

3.1 Amplitude responses of maximum-power and amplitude-equalizing combiners during dispersive fading

The transfer function of the multipath medium as seen by the main and diversity antennas is expressed as:

$$\bar{H}_M(j\omega, t) = 1 + b(t)e^{-j\omega\tau(t)} \tag{21}$$

and

$$\bar{H}_D(j\omega, t) = 1 + b(t)e^{-j\omega[\tau(t)+\tau'(t)]}, \tag{22}$$

where the subscripts M and D refer to the main and diversity antennas, respectively. Assuming a circular trajectory for the delayed wavefront, $\tau'(t)$ is approximated by:

$$\tau'(t) \approx h\left\{\frac{6\tau(t)}{cd}\right\}^{1/2}, \tag{23}$$

where h, d, and c denote antenna separation, hop length, and speed-of-light in air, respectively. Having calculated the state of the channel from eqs. (21) through (23), for given $b(t)$ and $\tau(t)$ values, the computer program then computes $V(\omega, t)$, $\delta(\omega, t)$, and $\psi(\omega, t)$, as defined by eqs. (37) through (39) of the appendix. The response of the phase-control loop of Fig. 2 is then evaluated in both the maximum-power and equalizing phase-control modes. In the equalizing mode, the narrowband filters (see Fig. 3) are assumed ideal, with ω_l, ω_r, and $\Delta\omega$ set at $\omega_c - B/4$, $\omega_c + B/4$, and $B/4$, respectively, with $B/2\pi$ denoting the channel bandwidth (in Hz) and ω_c the channel center frequency. With these filter settings, the equalizing-combiner algorithm performs maximum-power combining over the entire upper or lower half of the channel.

The computer simulations were repeated with other combinations of $\Delta\omega$, ω_l, and ω_r to parametrically investigate the effect of these filter

settings on the equalizing-combiner response. For some particular dispersive channel conditions, the equalizing-combiner response varied for different $\Delta\omega$, ω_l, and ω_r values. On an overall basis, however, the improvement afforded by the equalizing combiner was found insensitive to these filter parameters as long as ω_l and ω_r were chosen reasonably close to the channel edges.

For each simulated channel condition, two phase shifter corrections, $\theta_M(t)$ and $\theta_E(t)$, corresponding to the maximum-power and equalizing phase-control loops, respectively, were calculated. Then, effective transfer functions were formed, relating the maximum-power and equalizing-combiner output signals to the transmitted signal. The effective transfer functions generated by the maximum-power and equalizing combiners are expressed by

$$\bar{E}_M(j\omega, t) \equiv \frac{1}{\sqrt{2}} [\bar{H}_M(j\omega, t) + \bar{H}_D(j\omega, t)e^{j\theta_M(t)}] \tag{24}$$

and

$$\bar{E}_E(j\omega, t) \equiv \frac{1}{\sqrt{2}} [\bar{H}_M(j\omega, t) + \bar{H}_D(j\omega, t)e^{j\theta_E(t)}], \tag{25}$$

respectively, where the factor $1/\sqrt{2}$ is required to satisfy power conservation constraints at the output of the summing hybrid of Fig. 1.

Representative combiner responses, $\bar{E}_M(j\omega)$ and $\bar{E}_E(j\omega)$, are shown in Figs. 4 and 5. In Fig. 4, both transfer functions, $\bar{H}_M(j\omega)$ and $\bar{H}_D(j\omega)$, as seen by the main and diversity antennas respectively, contain a 40-dB fade notch within the channel bandwidth. The response of the maximum-power combiner, as shown, contains a substantial amount of linear and quadratic amplitude distortion across the channel. Its group-delay response (not shown) is also severely distorted. Unlike the maximum-power combiner, the equalizing-combiner amplitude response is flat (to within 1 dB) across the entire channel. The group-delay response of the equalizing combiner (not shown) is also flat across the channel.

Figure 5 shows a channel condition where only one antenna sees a transfer function with an inband notch. As with the situation of Fig. 4, here too, the maximum-power combiner suffers from linear and quadratic amplitude distortions. Note again the almost ideally flat response of the equalizing combiner. Figures 4 and 5 are typical of most simulated channel conditions where one or both antennas experience fade notches well within the channel bandwidth. There are channel conditions, however, where both antenna signals are affected by fade notches that fall outside the channel bandwidth, both below or above the channel-center frequency. These channel conditions produce a predominantly linear amplitude distortion in the channel, accompa-

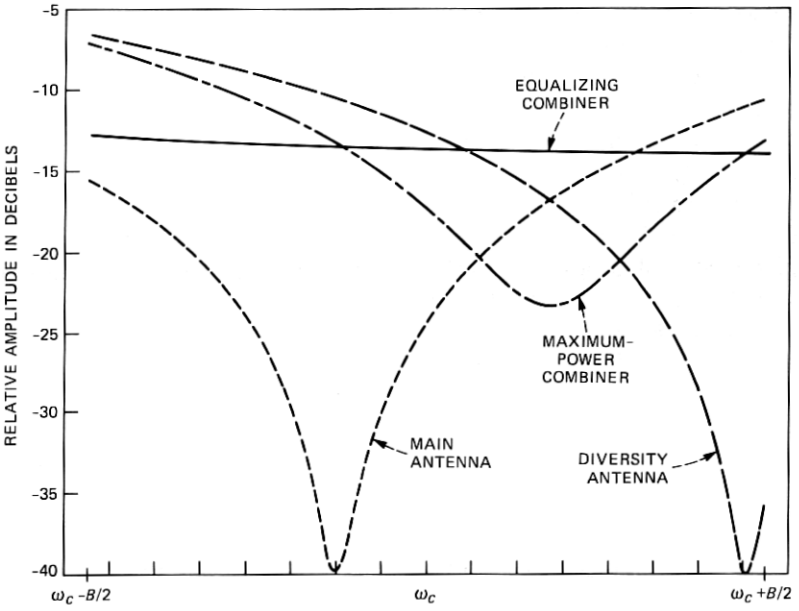

Fig. 4—Combiner response to a dispersive channel condition generated by $b = 0.99$ and $\tau = 2.4183$ ns. The channel bandwidth $= B/2\pi = 30$ MHz.

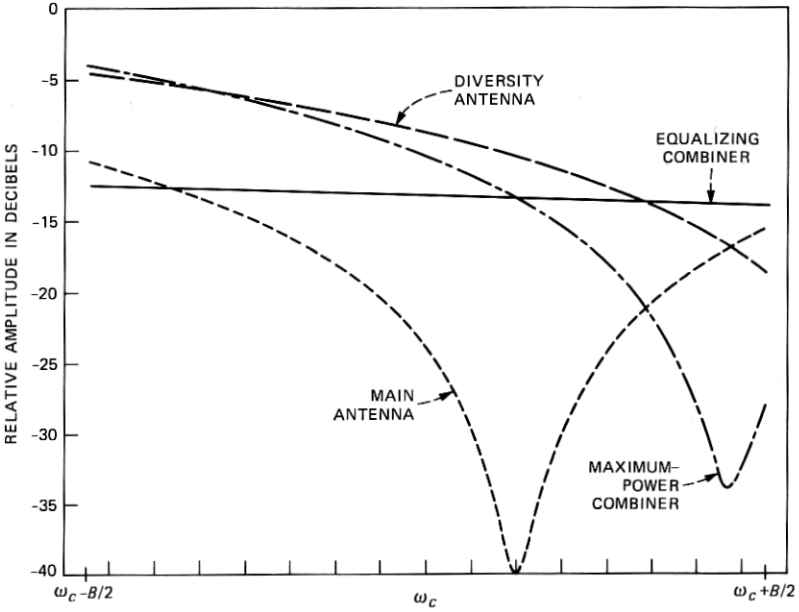

Fig. 5—Combiner response to a dispersive channel condition generated by $b = 0.99$ and $\tau = 2.4151$ ns. The channel bandwidth $= B/2\pi = 30$ MHz.

nied by negligible phase dispersion, since the phase dispersion produced by a fade is concentrated in the vicinity of the fade notch. In response to such a channel condition, the equalizing-combiner output signal can be only marginally better than that of the maximum-power combiner since the inband phase dispersion, required by the equalizing combiner to achieve amplitude equalization, does not exist. Unfortunately, the channel condition described above has a higher probability of occurrence than those depicted in Figs. 4 and 5 (where at least one antenna signal contains a fade notch within the channel) since the channel bandwidth is typically a small fraction of the period $1/\tau$, or $1/(\tau + \tau')$, with which the fade notches repeat. As a result, the reduction in outage time afforded by the equalizing combiner, relative to that of the maximum-power combiner, is limited to relatively small values, as we will see in the following section.

3.2 Relative improvement factor of amplitude-equalizing combiner

In this section, a method of calculating regions on the $\lambda - \tau$ plane ($\lambda \equiv 1 - b$, denoting the fade depth at the fade notch) corresponding to system outage is described. Several outage regions corresponding to the maximum-power and equalizing combiners are calculated. Integration over these regions (having assumed some joint probability-density function for the variables λ, τ) allows us to compare the performance of the two combiner algorithms and associate a relative improvement factor with the equalizing-combiner algorithm. The relative-improvement factor of the equalizing combiner is shown to be highly dependent on the assumed probability-density function associated with the multipath delay τ, and on the expected value of the multipath delay, τ_0. The relative improvement factor of the equalizing combiner is calculated and plotted as a function of τ_0 for two assumed probability-density functions of τ.

The computer simulation described in the previous section was extended to statistically evaluate the relative performance of the maximum-power and amplitude-equalizing combiners with respect to dispersive channel conditions of at least 6-dB peak-to-peak amplitude distortion in the channel. The threshold value of 6-dB peak-to-peak amplitude distortion was chosen for simplicity, since the accumulated time at this, or greater dispersive levels, has been found strongly correlated with the total outage time of high-speed digital signals.[2,8]

Starting from a value of τ that produces a fade notch at the center of the main antenna spectrum, as determined by

$$\tau = \frac{2n + 1}{2f_c}, f_c = \frac{\omega_c}{2\pi}, n = 0, 1, 2, \cdots,$$

values of λ satisfying the outage condition at the maximum-power

and/or equalizing-combiner outputs are determined. Then, by perturbing each initial value of τ, the fade notch is moved by a small amount (2-MHz increment) and b is varied again until all λ values satisfying the outage condition at the new setting are found. Perturbations in τ continue until a frequency band of ±100 MHz around the band center has been examined. Following this procedure, the first five outage regions, corresponding to $n = 13$ through 17, were evaluated for the maximum-power and amplitude-equalizing combiners. No outage regions were found for $n = 0$ through 12 and $n = 18$ through 25. The effect of outage regions corresponding to values of n greater than 25 were neglected in this study. The first five outage regions that were evaluated are shown in Figs. 6 through 10. On each figure, the value of n and the value of τ generating the fade notch at the center of the

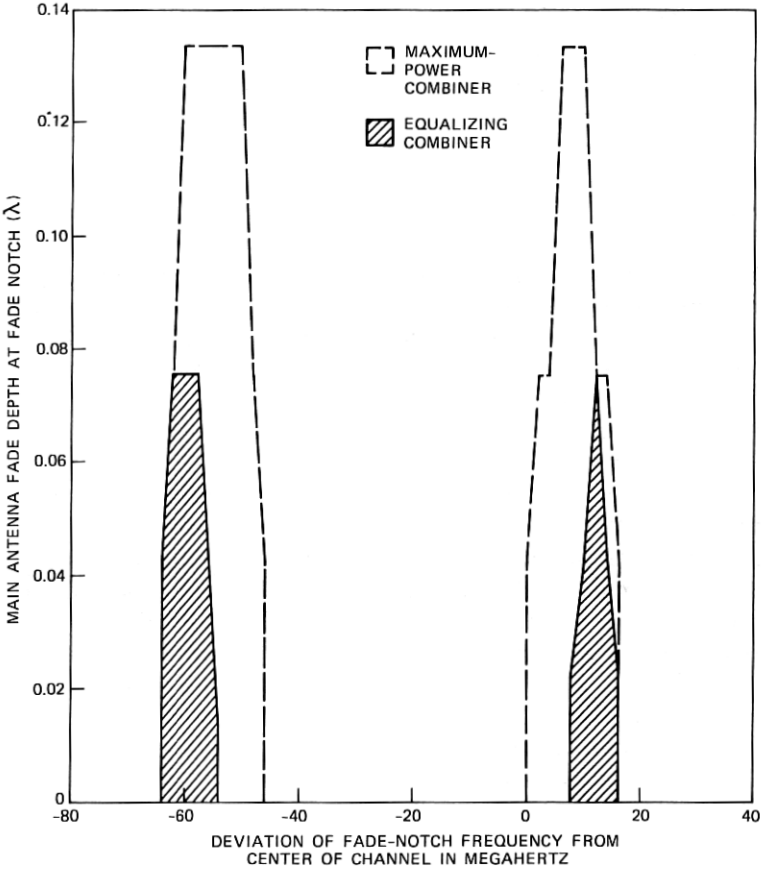

Fig. 6—Maximum-power and equalizing-combiner outage regions for $n = 13$ and $\tau = 2.25$ ns.

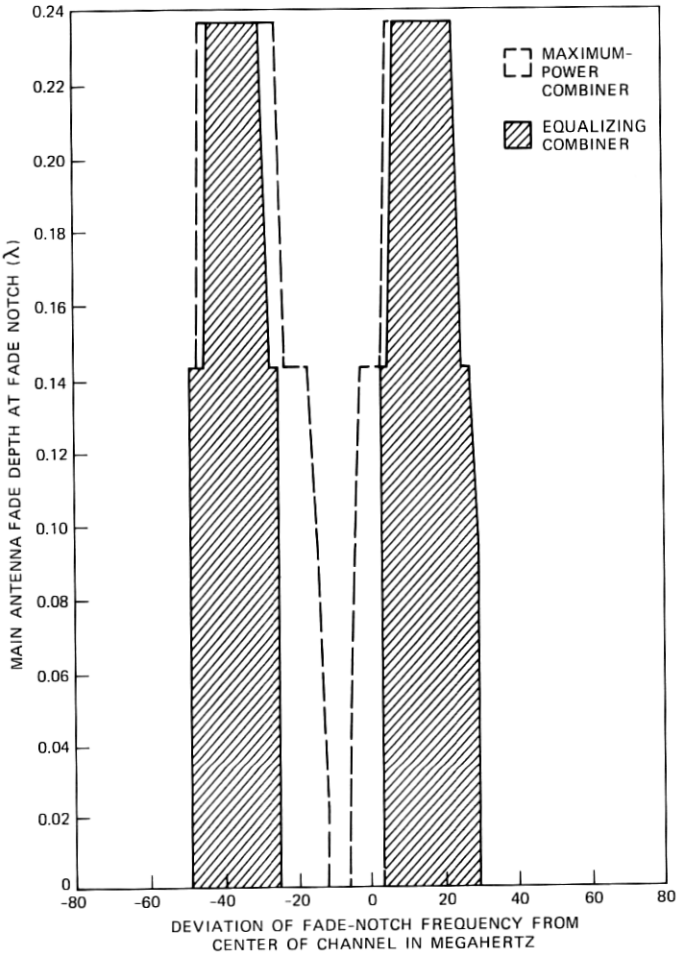

Fig. 7—Maximum-power and equalizing-combiner outage regions for $n = 14$ and $\tau = 2.4167$ ns.

main antenna spectrum are shown. The curves show fade-notch depth as a function of fade-notch location for the main antenna, which results in system outage as defined by the 6-dB amplitude distortion on the combiner outputs. Note that in every case the equalizing-combiner outage region (the shaded area) is totally contained within the maximum-power combiner outage region, which is bounded by the dashed curve. From this simple observation we conclude that the equalizing combiner is outperforming the maximum-power combiner in maintaining reduced levels of channel distortion. The performance improvements, however, are not large. As we can see in Figs. 7, 8, and 9, which contain the larger maximum-power combiner outage regions, the

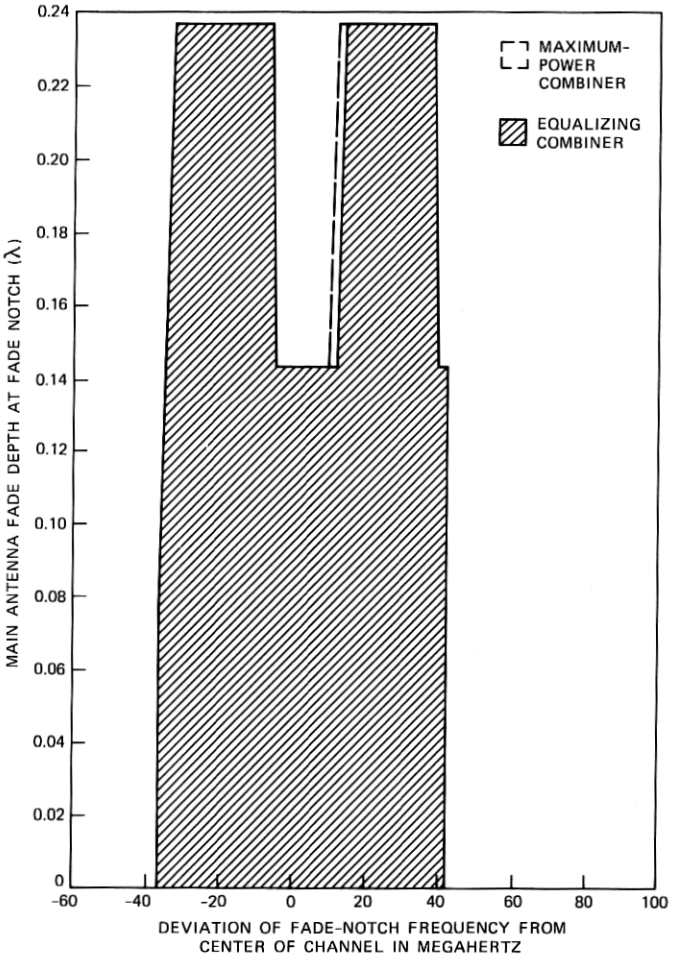

Fig. 8—Maximum-power and equalizing-combiner outage regions for $n = 15$ and $\tau = 2.5833$ ns.

equalizing-combiner outage regions are comparable to those of the maximum-power combiner. Specifically, Fig. 8 shows almost identical outage regions for the two combiners. Close examination of the channel conditions responsible for the outage regions of Fig. 8 reveals very closely correlated fading between the two antenna spectra (i.e., almost simultaneous frequency selective fading). On all other figures, the equalizing combiner outage regions are due to channel conditions that contain little or no inband phase distortion (i.e., fade notches very close to, or completely outside, the channel limits).

To calculate an outage probability for the maximum-power and

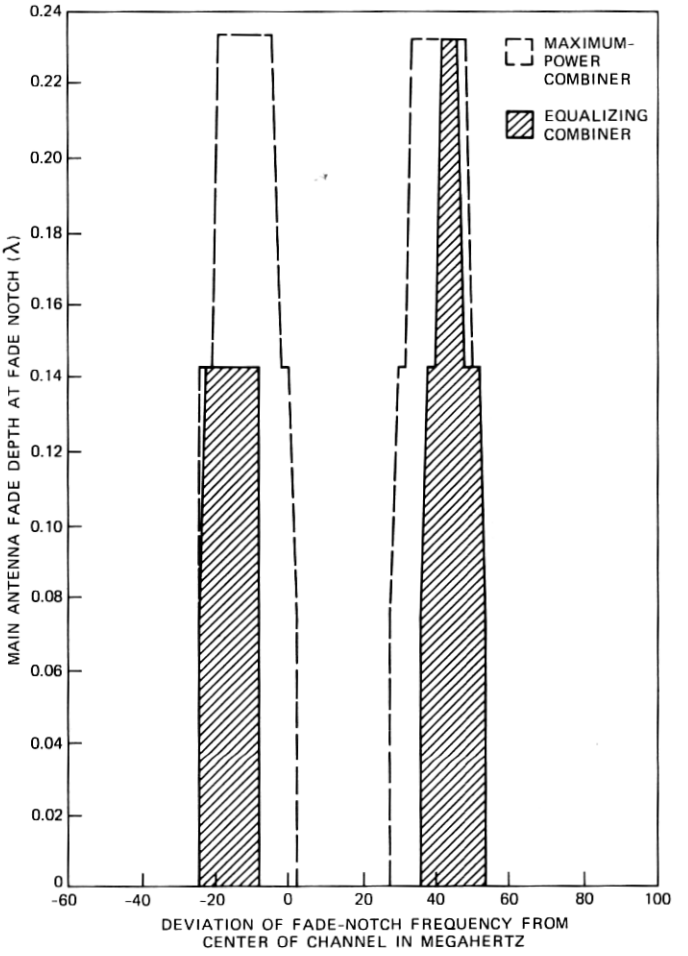

Fig. 9—Maximum-power and equalizing-combiner outage regions for $n = 16$ and $\tau = 2.75$ ns.

equalizing combiners, their corresponding outage regions must be weighted by the joint probability-density function $p_{\tau,\lambda}(\tau, \lambda)$, followed by integration over the appropriate limits and summation of all weighted contributions from all outage regions. Accordingly, the probability of outage of the maximum-power combiner can be expressed as:

$$P_M = \sum_{n=13}^{17} \int_{\tau_M^-(n)}^{\tau_M^+(n)} \int_0^{\lambda_M(n,\tau)} p_{\tau,\lambda}(\tau, \lambda) d\lambda d\tau, \tag{26}$$

where the subscript M stands for maximum-power combiner, the limits

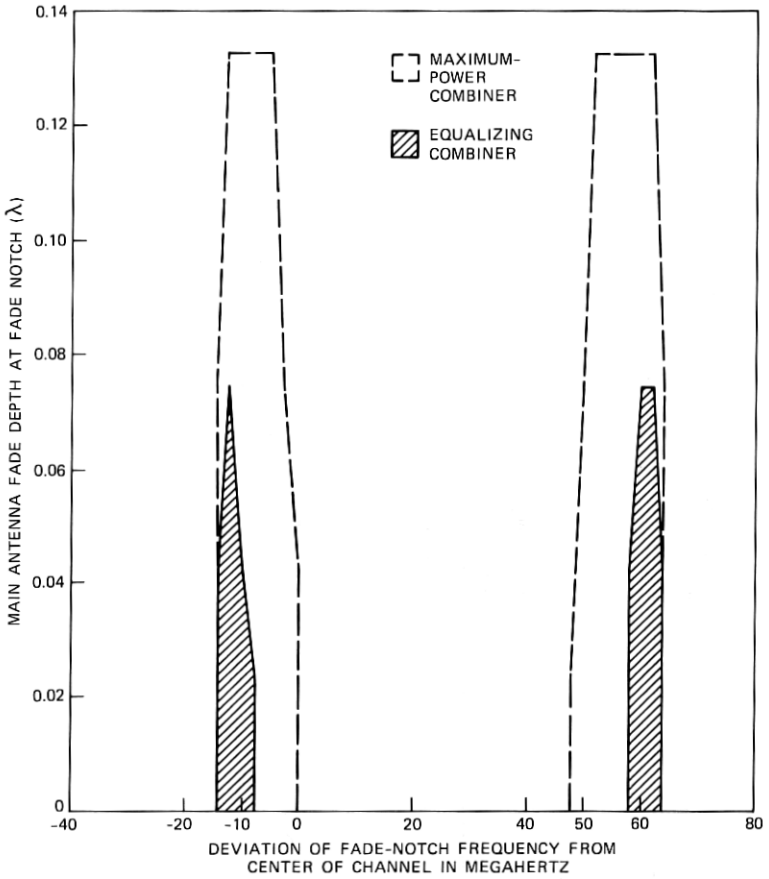

Fig. 10—Maximum-power and equalizing-combiner outage regions for $n = 17$ and $\tau = 2.9167$ ns.

$\tau_M^-(n)$ and $\tau_M^+(n)$ define the range of variation of τ (for a particular value of n) inside which the outage region lies, and $\lambda_M(n, \tau)$ denotes the minimum fade-depth resulting in outage as a function of τ, for a specific value of n. Similarly, the probability of outage of the equalizing combiner can be evaluated from:

$$P_E = \sum_{n=13}^{17} \int_{\tau_E^-(n)}^{\tau_E^+(n)} \int_0^{\lambda_E(n,\tau)} p_{\tau,\lambda}(\tau, \lambda) d\lambda d\tau. \tag{27}$$

Using eqs. (26) and (27) we define an equalizing-combiner improvement factor, I, over the maximum-power combiner,

$$I \equiv \frac{P_M}{P_E}. \tag{28}$$

To simplify the calculations in evaluating eq. (28) we assume statistical independence between the fade depth λ and delay τ, allowing the joint probability-density function to be written as

$$p_{\tau,\lambda}(\tau, \lambda) = p_\tau(\tau) p_\lambda(\lambda). \tag{29}$$

Two probability-density functions of τ are considered.[3,15,16] The exponentially distributed

$$p_\tau^{(e)}(\tau) = \frac{1}{\tau_0} e^{-\frac{\tau}{\tau_0}}, \qquad \tau \geq 0, \tag{30}$$

and the Gaussian distributed

$$p_\tau^{(G)}(\tau) = \frac{2}{\pi\tau_0} e^{-\frac{\tau^2}{\pi\tau_0^2}}, \qquad \tau \geq 0, \tag{31}$$

where in both cases τ_0 denotes the expected value of τ. The probability-density function of λ is assumed of the form[3,15]

$$p_\lambda(\lambda) = \frac{\rho}{1 - e^{-\rho}} e^{-\rho\lambda}, \qquad 0 \leq \lambda \leq 1, \tag{32}$$

with $\rho = 10$.

The equalizing-combiner improvement factor, I, is evaluated for the two joint probability-density functions, $p_\lambda(\lambda)p_\tau^{(e)}(\tau)$ and $p_\lambda(\lambda)p_\tau^{(G)}(\tau)$, as a function of the expected delay difference τ_0. The results are shown on Fig. 11. Note the strong dependence of I on τ_0 for the curve corresponding to $p_\tau(\tau) = p_\tau^{(G)}(\tau)$. This is due to the Guassian nature of $p_\tau^{(G)}(\tau)$ which, for small values of τ_0, provides smaller weighting factors for the large outage regions (of Fig. 7, 8, and 9) than does $p_\tau^{(e)}(\tau)$. Also,

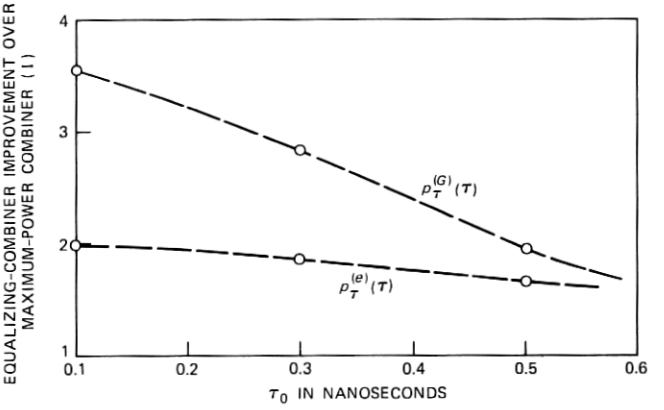

Fig. 11—Equalizing-combiner improvement factor as a function of the expected value of τ.

note the change in improvement factor, for a given value of τ_0, as a function of the two assumed probability-density functions of τ. This is to be expected since the ratio of the outage areas of the maximum-power combiner to those of the equalizing combiner varies considerably for Figs. 6 through 10. Thus, the particular weighting given to the areas of each figure, as determined by the assumed probability-density function of τ, will control the outcome of I. To illustrate this point further, we consider a delay difference τ, which is uniformly distributed between $\tau = 2.8$ and 3.1 ns, and zero outside this range. That is, we assume:

$$p_\tau(\tau) \equiv p_\tau^{(u)}(\tau) = \begin{cases} \text{constant}, & \text{for } 2.8 \le \tau \le 3.1 \text{ ns}, \\ 0, & \text{otherwise}. \end{cases} \tag{33}$$

With this probability-density function we calculate an equalizing-combiner improvement factor of five relative to that of the maximum-power combiner, since only the outage region of Fig. 10 contributes (equalizing-combiner improvement factors of this magnitude have recently been observed on a reflective microwave radio path over water[7]). By a similar argument, if τ is assumed uniformly distributed between $\tau = 2.4$ and 2.7 ns, with zero probability of assuming a value outside this range, the equalizing-combiner improvement factor reduces to approximately unity.

From the above considerations it becomes apparent that the delay-difference statistics used in the two-ray model will play a major role in determining the equalizing-combiner performance relative to that of the maximum-power combiner. Regardless of the delay-difference statistics, however, our analysis predicts only moderate outage reductions to be gained from converting a maximum-power combiner to an equalizing combiner. This suggests that an amplitude-slope equalizer may still be required following the equalizing combiner to bring the outage time of high-speed digital signals to levels below long-haul outage objectives. Nevertheless, the equalizing combiner's ability to mitigate quadratic as well as linear amplitude distortions, during highly dispersive channel conditions, will contribute to enhancing the reliability and robustness of high-speed digital radio systems.

IV. ACKNOWLEDGMENTS

I am indebted to L. A. Palazzo for the great deal of support he provided in generating the computer simulations and to T. L. Osborne for his constant encouragement. I am also grateful to W. D. Rummler for his many useful suggestions.

REFERENCES

1. A. J. Giger and W. T. Barnett, "Effects of Multipath Propagation on Digital Radio," Paper 46.7, Int. Conf. on Commun., June 14–18, 1981, Denver, Colorado.

2. C. W. Lundgren and W. D. Rummler, "Digital Radio Outage Due to Selective Fading—Observation vs. Prediction from Laboratory Simulation," B.S.T.J., *58*, No. 5 (May–June 1979), pp. 1073–100.
3. W. C. Jakes, Jr., "An Approximate Method to Estimate an Upper Bound on the Effect of Multipath Delay Distortion on Digital Transmission," IEEE Trans. on Commun., *COM-27*, No. 1 (January 1979), pp. 76–81.
4. C. W. Anderson, S. G. Barber, and R. N. Patel, "The Effect of Selective Fading on Digital Radio," IEEE Trans. on Commun., *COM-27*, No. 12 (December 1979), pp. 1870–5.
5. W. T. Barnett, "Multipath Fading Effects on Digital Radio," IEEE Trans. on Commun., *COM-27*, No. 12 (December 1979), pp. 1842–8.
6. S. Komaki, I. Horikawa, K. Morita, and Y. Okamoto, "Characteristics of a High Capacity 16 QAM Digital Radio System in Multipath Fading," IEEE Trans. on Commun., *COM-27*, No. 12 (December 1979), pp. 1854–61.
7. T. Murase, K. Morita, and S. Komaki, "200 Mb/s 16-QAM Digital Radio System with New Countermeasure Techniques for Multipath Fading," Paper 46.1, Int. Conf. on Commun., June 14–18, 1981, Denver, Colorado.
8. Y. Y. Wang, "Simulation and Measured Performance of a Space Diversity Combiner for 6 GHz Digital Radio," IEEE Trans. on Commun., *COM-27*, No. 12 (December 1979), pp. 1896–907.
9. P. Hartmann and B. Bynum, "Design Considerations for an Extended Range Adaptive Equalizer," Paper 46.5, Int. Conf. on Commun., June 14–18, 1981, Denver, Colorado.
10. W. T. Barnett, C. W. Lundgren, Jr., W. D. Rummler, and Y. Y. Wang, "Equalizing Signal Combiner," U. S. Patent 4,261,056, applied for July 16, 1979, issued April 7, 1981.
11. S. Komaki, Y. Okamoto, and K. Tajima, "Performance of 16-QAM Digital Radio System Using New Space Diversity," Paper 52.2, Int. Conf. on Commun., June 8–12, 1980, Seattle, Washington.
12. W. D. Rummler, "A New Selective Fading Model: Application to Propagation Data," B.S.T.J., *58*, No. 5 (May–June 1979), pp. 1037–71.
13. H. Miedema, unpublished work.
14. K. L. Seastrand, Jr., "Space Diversity Receiver with Combined Step and Continuous Pase Control," U. S. Patent 4,160,952, applied for May 12, 1978, issued July 10, 1979.
15. L. J. Greenstein and V. K. Prabhu, "Analysis of Multipath Outage with Applications to 90 Mbit/s PSK Systems at 6 and 11 GHz," IEEE Trans. on Commun., *COM-27*, No. 1 (January 1979), pp. 68–75.
16. M. Emshwiller, "Characterization of the Performance of PSK Digital Radio Transmission in the Presence of Multipath Fading," Int. Conf. on Commun., ICC 1978.
17. L. W. Pickering and J. K. DeRosa, "Refractive Multipath Model for Line-of-Sight Microwave Relay Links," IEEE Trans. on Commun., *COM-27*, No. 8 (August 1979), pp. 1174–82.
18. O. Sasaki and T. Akiyama, "Multipath Delay Characteristics on Line-of-Sight Microwave Radio System," IEEE Trans. on Commun., *COM-27*, No. 12 (December 1979), pp. 1876–86.
19. M. Ramadan, "Availability Prediction of 8 PSK Digital Microwave Systems During Multipath Propagation," IEEE Trans. on Commun., *COM-27*, No. 12 (December 1979), pp. 1862–9.

APPENDIX

Modulation of Combined-Signal Power

By modulating the phase of one antenna signal with a low-frequency sinsuoid, the combined-signal power over some arbitrary frequency interval, $\omega_1 \leq \omega \leq \omega_2$ (spanning all or some portion of the channel) will be modulated periodically. In this appendix, we expand the periodic modulation of the combined-signal power in a Fourier series and show that, in the absence of channel dispersion, the fundamental component of the expansion is proportional to the sine of the phase difference between the antenna signals at the inputs of the summing hybrid (see

Fig. 1). During dispersive channel conditions, we show that the fundamental component of the expansion is a weighted average of the sine of the phase difference between the antenna signals at the inputs of the summing hybrid. We thus show that the fundamental component of the combined-signal power modulation can be used as a measure of phase-lead or phase-lag of one antenna signal relative to the other.[13]

Let $\bar{R}_M(j\omega, t)$ and $\bar{R}_D(j\omega, t)$ denote the complex spectral densities received by the main and diversity antennas, respectively, in response to a transmitted signal $s(t)$, with complex spectral density $\bar{S}(j\omega)$. Denoting the transmission-medium transfer function by $\bar{H}_M(j\omega, t)$ and $\bar{H}_D(j\omega, t)$, as seen by the main and diversity antennas, respectively, we can write

$$\bar{R}_M(j\omega, t) = \bar{H}_M(j\omega, t)\bar{S}(j\omega)e^{-j\omega T_0} \tag{34}$$

and

$$\bar{R}_D(j\omega, t) = \bar{H}_D(j\omega, t)\bar{S}(j\omega)e^{-j\omega T_0}, \tag{35}$$

where the delay T_0 denotes the line-of-sight propagation delay of the radio link. The dependence of $\bar{H}_M$ and $\bar{H}_D$ on t allows for variations in the transmission-medium transfer function during anomalous propagation conditions (i.e., during multipath fading). However, in writing eqs. (34) and (35) the transmission-medium transfer functions are assumed quasi-static with respect to the rate-of-change of $s(t)$. Defining,

$$\bar{S}(j\omega) \equiv S_0(\omega)e^{j\phi(\omega)}, \tag{36}$$

$$\bar{H}_M(j\omega, t) \equiv H(\omega, t)e^{j\eta(\omega,t)}, \tag{37}$$

$$\bar{H}_D(j\omega, t) \equiv \delta(\omega, t)H(\omega, t)e^{j\{\eta(\omega,t)+\psi(\omega,t)\}}, \tag{38}$$

and

$$V(\omega, t) \equiv H(\omega, t)S_0(\omega), \tag{39}$$

eqs. (34) and (35) can be rewritten as

$$\bar{R}_M(j\omega, t) = V(\omega, t)e^{j\{\phi(\omega)+\eta(\omega,t)-\omega T_0\}} \tag{40}$$

and

$$\bar{R}_D(j\omega, t) = \delta(\omega, t)V(\omega, t)e^{j\{\phi(\omega)+\eta(\omega,t)+\psi(\omega,t)-\omega T_0\}}. \tag{41}$$

The quantities $H(\omega, t)$ and $\eta(\omega, t)$ appearing in eq. (37) represent the amplitude and phase transfer functions associated with the dynamic transmission medium. The parameter $\delta(\omega, t)$ of eq. (38) denotes the voltage ratio of the diversity to the main antenna signal as a function of frequency and time, and $\psi(\omega, t)$ describes the phase of the spectrum

received by the diversity antenna referenced to the phase of the spectrum received by the main antenna. Both parameters $\delta(\omega, t)$ and $\psi(\omega, t)$ must be frequency- as well as time-dependent since during anomalous propagation periods the spectral densities received by the two antennas will, in general, differ by a complex, frequency-dependent, time-varying factor.

Assuming ideal waveguide systems and ideal phase-shifting elements, the spectral densities at the inputs of the summing hybrid (Fig. 1) can be expressed as:

$$\bar{R}'_M(j\omega, t) = \bar{R}_M(j\omega, t)e^{-j\omega\tau_{WG}} \tag{42}$$

and

$$\bar{R}'_D(j\omega, t) = \bar{R}_D(j\omega, t)e^{j\{\theta+\alpha\sin\omega_m t-\omega\tau_{WG}\}}, \tag{43}$$

where τ_{WG} denotes the waveguide propagation delay (assumed the same for both equalized waveguide systems), and $\theta + \alpha \sin \omega_m t$ represents the instantaneous frequency-independent phase shift introduced into the diversity signal by the phase modulator/phase shifter combination. It can be seen from eqs. (40) through (43) that at the inputs of the summing hybrid the instantaneous phase difference between the diversity antenna spectrum and the main antenna spectrum is $\psi(\omega, t) + \theta + \alpha \sin \omega_m t$. The combined signal spectrum can now be expressed as

$$\begin{aligned}\bar{R}_C(j\omega, t) \equiv V_C(\omega, t)e^{j\phi_C(\omega,t)} &= \frac{1}{\sqrt{2}}[\bar{R}'_M(j\omega, t) + \bar{R}'_D(j\omega, t)] \\ &= \frac{1}{\sqrt{2}}[1 + \delta(\omega, t)e^{j\{\psi(\omega,t)+\theta+\alpha\sin\omega_m t\}}] \\ &\quad \cdot V(\omega, t)e^{j\{\phi(\omega)+\eta(\omega,t)-\omega(T_0+\tau_{WG})\}}.\end{aligned} \tag{44}$$

Expanding the exponential function inside the square brackets in terms of sine and cosine functions, followed by an expansion of $\sin\{\alpha \sin \omega_m t\}$ and $\cos\{\alpha \sin \omega_m t\}$ in terms of Bessel functions, yields (after some algebraic manipulation),

$$\begin{aligned}&V_C^2(\omega, t) \\ &\quad = \frac{1}{2} V_{co}^2(\omega, t)[1 - m_1(\omega, t)\sin \omega_m t + m_2(\omega, t)\cos 2\omega_m t \cdots],\end{aligned} \tag{45}$$

where

$$V_{co}^2(\omega, t) \equiv \delta(\omega, t)V^2(\omega, t)[\delta(\omega, t) + \frac{1}{\delta(\omega, t)} + 2J_0(\alpha)\cos \mu(\omega, t)], \tag{46}$$

$$m_1(\omega, t) \equiv \frac{4J_1(\alpha)\sin \mu(\omega, t)}{\delta(\omega, t) + \dfrac{1}{\delta(\omega, t)} + 2J_0(\alpha)\cos \mu(\omega, t)}, \tag{47}$$

$$m_2(\omega, t) \equiv \frac{4J_2(\alpha)\cos \mu(\omega, t)}{\delta(\omega, t) + \dfrac{1}{\delta(\omega, t)} + 2J_0(\alpha)\cos \mu(\omega, t)}, \cdots, \tag{48}$$

$$\mu(\omega, t) \equiv \psi(\omega, t) + \theta, \tag{49}$$

and J_0, J_1, J_2 denote Bessel functions of the first kind. Note that the modulation component, $m_1(\omega, t)$, at the fundamental frequency of phase modulation, ω_m, is proportional to the sine of the average phase difference $\mu(\omega, t)$. [The average phase difference is obtained by averaging the instantaneous phase difference, $\psi(\omega, t) + \theta + \alpha \sin \omega_m t$, over one period of $\alpha \sin \omega_m t$. Over this time interval the term $\psi(\omega, t) + \theta$ is assumed fixed.] Furthermore, since α (the magnitude of phase modulation) is typically kept small, $0 < \alpha \ll \pi/2$, $J_0(\alpha)$ will be positive and less than unity. Also, the denominator term of $m_1(\omega, t)$ will always be positive since $-2 < 2J_0(\alpha)\cos \mu(\omega, t) < 2$ for all $\mu(\omega, t)$, given that $0 < \alpha \ll \pi/2$, and $\delta(\omega, t) + 1/\delta(\omega, t) \geq 2$ for all $\delta(\omega, t)$, $0 \leq \delta(\omega, t_0) \leq \infty$. Therefore, the sign of $m_1(\omega, t)$ will indicate whether, at a particular frequency and point in time, the phase of the diversity spectrum leads or lags the phase of the main antenna spectrum.

The combined-signal power contained in the frequency interval $\omega_1 \leq \omega \leq \omega_2$ can be expressed as:

$$p_C(t) = \frac{1}{\pi} \int_{\omega_1}^{\omega_2} V_C^2(\omega, t) d\omega. \tag{50}$$

Substituting eq. (45) into eq. (50) and manipulating terms results in:

$$p_C(t) = p_0(t)[1 - m_1'(t)\sin \omega_m t + m_2'(t)\cos 2\omega_m t \cdots] \tag{51}$$

where

$$p_0(t) \equiv \frac{1}{2\pi} \int_{\omega_1}^{\omega_2} V_{co}^2(\omega, t) d\omega, \tag{52}$$

$$m_1'(t) \equiv \frac{\displaystyle\int_{\omega_1}^{\omega_2} m_1(\omega, t) V_{co}^2(\omega, t) d\omega}{\displaystyle\int_{\omega_1}^{\omega_2} V_{co}^2(\omega, t) d\omega}, \tag{53}$$

$$m_2'(t) \equiv \frac{\int_{\omega_1}^{\omega_2} m_2(\omega, t) V_{co}^2(\omega, t) d\omega}{\int_{\omega_1}^{\omega_2} V_{co}^2(\omega, t) d\omega}, \quad \cdots . \tag{54}$$

Note that $m_1'(t)$ represents a weighted average of $m_1(\omega, t)$ over the interval $\omega_1 \leq \omega \leq \omega_2$, where the weighting function $V_{co}^2(\omega, t)$ is proportional to the average combined-signal power spectral density.

In the absence of channel dispersion (i.e., flat fading, or no fading at all) μ and m_1 become frequency independent, thus making m_1' identically equal to m_1 [see eq. (53)]. Since m_1 is proportional to $\sin \mu$, the sign of m_1' can be used to determine whether μ represents a positive or negative angle (phase lead or phase lag of the diversity signal with respect to the main antenna signal) during dispersion-free periods. When the channel is dispersive, however (i.e., during periods of frequency-selective fading), the phase difference between the two spectra becomes frequency-dependent and m_1' will reflect a weighted average of $\sin \mu$ over the interval $\omega_1 \leq \omega \leq \omega_2$. This can be seen by substituting eqs. (46) and (47) into eq. (53). Doing so, we find

$$m_1'(t) = \frac{4J_1(\alpha) \int_{\omega_1}^{\omega_2} \delta(\omega, t) V^2(\omega, t) \sin \mu(\omega, t) d\omega}{\int_{\omega_1}^{\omega_2} V_{co}^2(\omega, t) d\omega}, \tag{55}$$

where the weighting function $\delta(\omega, t) V^2(\omega, t)$ is the magnitude of the product of the received spectral densities. In Section 2.1 we show that when $\omega_1 \leq \omega \leq \omega_2$ covers the entire channel bandwidth and $m_1'(t)$ is used in a feedback arrangement to control the phase-shifter value θ, maximum-power combining of the received signals results for all channel conditions.